communications biology

Article

https://doi.org/10.1038/s42003-025-07571-5

NLRP7 maintains the genomic stability during early human embryogenesis via mediating alternative splicing

Check for updates

Zhongliang Chen [1,2,3,9], Liangxia Jiang [4,5,9], Min Su[2,3,6], Qibing Zeng[7,8], Peng Luo [7,8] ✉ & Liangzhao Chu [1] ✉

Genomic instability is the main cause of abnormal embryo development and abortion. NLRP7 dysfunctions affect embryonic development and lead to Hydatidiform Moles, but the underlying mechanisms remain largely elusive. Here, we show that *NLRP7* knockout affects the genetic stability, resulting in increased DNA damage in both human embryonic stem cells and blastoids, making embryonic cells in blastoids more susceptible to apoptosis. Mechanistically, NLRP7 can interact with factors related to alternative splicing and DNA damage response, including DDX39B, PRPF8, THRAP3 and PARP1. Moreover, *NLRP7* dysfunction leads to abnormal alternative splicing of genes involved in homologous recombination in human embryonic stem cells, Such as *Brca1* and *Rad51*. These results indicate that NLRP7-mediated Alternative splicing is potentially required for the maintenance of genome integrity during early human embryogenesis. Together, this study uncovers that NLRP7 plays an essential role in the maintenance of genetic stability during early human embryonic development by regulating alternative splicing of homologous recombination-related genes.

Early embryonic cells are susceptible to internal and external environmental factors, which affect genetic stability and may lead to DNA damage or aneuploidy[1,2]. More than 50% of preimplantation embryos exhibit chromosomal abnormalities, which compromise their implantation[3]. This may be related to the special cell cycle feature of early embryonic cells[4]. In addition, early embryos are highly sensitive to DNA double-strand breaks (DSBs), even a small number of DSBs may induce apoptosis and potentially lead to early embryo death[5]. Furthermore, although the types and numbers of cells that make up the early embryo are limited, there is significant heterogeneity among these cells. The tolerance of different cells within early embryos to abnormal chromosomes varies significantly. For example, Compared to other cells, Epiblast cells at the gastrulation stage in mice were extremely sensitive to DNA damage induced by ray and proned to apoptosis[6]. The same characteristics had also been found in human embryonic stem cells (hESCs) derived from the epiblast[7]. Thus, early embryonic cells may be in a heightened state of vigilance, and as soon as chromosomal abnormalities are detected, these cells are promptly eliminated. This selective elimination likely serves as a self-protection mechanism during embryonic development, aimed at preventing the continued development of embryos with abnormal chromosomes. Despite this, the precise mechanisms that trigger apoptosis in embryonic cells with chromosomal abnormalities remain largely unknown.

Alternative splicing (AS) is a crucial mechanism for gene expression regulation, enabling a single gene to produce multiple unique mRNAs isoforms and playing an important role in many biological processes[8,9], especially during the development of early embryos[10–12]. In addition, AS also frequently occurs during the expression of genes involved in DNA damage repair, cell cycle control, and apoptosis. A genome-wide siRNA screening study revealed that the absence of many splicing factors led to increased DNA damage[13]. Furthermore, some splicing factors, such as Serine/arginine-rich splicing factors (SRSFs), are multifunctional proteins that play a direct role in DNA repair. For example, inactivation of SRSF1 and SRSF3

[1]Department of Neurosurgery, The Affiliated Hospital of Guizhou Medical University, Guiyang, China. [2]Guizhou Province Key Laboratory of Regenerative Medicine, Guizhou Medical University, Guiyang, China. [3]Tissue Engineering and Stem Cell Experiment Center, Guizhou Medical University, Guiyang, China. [4]Department of Pathophysiology, School of Basic Medicine, Guizhou Medical University, Guiyang, China. [5]Guizhou Provincial Key Laboratory of Pathogenesis and Drug Research on Common Chronic Diseases, Guizhou Medical University, Guiyang, China. [6]Key Laboratory for Research on Autoimmune Diseases of Higher Education schools in Guizhou Province, Guizhou Medical University, Guiyang, China. [7]Key Laboratory of Environmental Pollution Monitoring and Disease Control, Ministry of Education, School of Public Health, Guizhou Medical University, Guiyang, China. [8]Collaborative Innovation Center for Prevention and Control of Endemic and Ethnic Regional Diseases Co-constructed by the Province and Ministry, Guizhou Medical University, Guiyang, China. [9]These authors contributed equally: Zhongliang Chen, Liangxia Jiang. ✉e-mail: luopeng@gmc.edu.cn; chulz_gmu@163.com

leads to genetic instability[14,15] and early embryonic developmental arrest[16]. Thus, there appears to be a close relationship between DNA damage, alternative splicing, and early embryonic development. However, the factors prevalent in embryonic cells that regulate alternative splicing remain to be elucidated.

NLRP7 is a member of NLRPs (Nucleotide-binding oligomerization domain, Leucine-rich Repeat, and Pyrin domain containing) family of cytoplasmic proteins, which is involved in the formation of inflammasomes, suggesting that it plays an important role in immunomodulatory processes[17]. In addition, NLRP7 is also expressed in human oocytes and early embryonic cells[18–20]. Mutations in *NLRP7* have been associated with hydatidiform mole (HM)[21], which is an abnormal pregnancy, characterized by placental overgrowth, while the embryonic development is severely abnormal or absent. Recurrent hydatidiform moles (RHMs) are defined by the occurrence of two or more molar pregnancies in the same patient. RHMs may be sporadic, occurring in a single individual in a family, or maybe familial as in biparental moles (BiCHM) that have both a maternal and a paternal contribution[22]. Mutations in *NLRP7* or *KHDC3L* genes, associated with maternal imprinting defects, have been involved in the development of RHM. Epigenetic studies in molar tissue from women carrying recessive *NLRP7* mutations have revealed aberrant DNA methylation profiles at a number of imprinted genes[23–26]. In addition to imprinting defects, abnormal inflammasome formation[27], cytokines release[28], and trophoblast differentiation[29] were also found to be related to HM. However, these studies primarily address how *NLRP7* mutations affect the proliferation, differentiation, and secretory function of trophoblasts (extraembryonic cells), leaving unclear how NLRP7 regulates early embryonic development and how its dysfunction contributes to human disease pathogenesis.

In the present study, we investigated the role of NLRP7 in maintaining genetic stability in human early embryonic cells and discovered that depletion of *NLRP7* resulted in DNA damage accumulation and apoptosis in hESCs and blastoids, and subsequently impaired blastoid development. Additionally, further studies demonstrated that NLRP7 interacted with factors involved in both AS and DNA damage response (DDR), including DDX39B, PRPF8, THRAP3, and PARP1, and its dysfunction disrupted the AS of homologous recombination (HR)-related genes, contributing to genetic instability and embryonic development defects.

Results

NLRP7 is required for maintenance of genomic DNA integrity in p-hESCs

The genetic instability is the main cause of abnormal embryonic development and miscarriage[30]. To determine whether NLRP7 was involved in maintaining the genetic stability in early human embryonic cells, we first analyzed RNA sequencing (RNA-seq) data of *NLRP7*-mutated human induced pluripotent stem cells (hiPSCs) derived from RHM patient' trophoblasts[29]. Kyoto Encyclopedia of Genes and Genomes (KEGG) analysis revealed that *NLRP7* mutation led to significant changes in DNA damage and the P53 signaling pathway (Fig. 1A). This suggested that NLRP7 might be involved in the maintenance of genetic stability in the early human embryonic cell.

To verify the analysis results, we used primed hESCs (p-hESCs) as a surrogate for epiblast cells, which share similar molecular and developmental properties with p-hESCs. By using CRISPR/Cas9 gene editing technology, the *NLRP7* knockout p-hESCs line (p-NLRP7$^{-/-}$) was successfully generated for subsequent experiments (Fig. 1B). We found that *NLRP7* knockout did not affect the expression of general pluripotent stem cells markers NANOG and OCT4 (Supplementary Fig. 1A), nor did it significantly alter the morphology of cell clones during long time culture in vitro. To investigate whether NLRP7 participates in maintaining DNA integrity in early human embryonic cells, we performed western blot and found that the expression of γH2A.X, a DNA damage marker, was elevated in the p-NLRP7$^{-/-}$ (Fig. 1B). This was corroborated by immunostaining, which revealed an increased number of γH2A.X positive cell in p-NLRP7$^{-/-}$ (Fig. 1C, D). Further confirmation came from single-cell gel electrophoresis analysis, showing that the p-NLRP7$^{-/-}$ exhibited more fragmented DNA and longer comet tails (Fig. 1E, F) compared to their wild-type counterparts. These findings demonstrate that *NLRP7* knockout leads to severe DNA damage, indicating that NLRP7 is crucial for maintaining the genome integrity of p-hESCs.

For proliferating cells, if DNA damage is not repaired in time, it may cause cell cycle arrest and even induce apoptosis. To this end, we next examined the effects of *NLRP7* deletion on cell cycle and apoptosis. We found that the proliferation of p-NLRP7$^{-/-}$ cells was not affected by BrdU labeling (Supplementary Fig. 1B, C), which was confirmed by fluorescence-activated cell sorting (FACS) analysis (Supplementary Fig. 1D). However, a significant increase in active caspase 3 was observed (Fig. 1G). These results indicated that *NLRP7* deletion induces apoptosis without impacting cell proliferation.

NLRP7 knockout accelerates differentiation of p-hESCs into trophoblasts

NLRP7 dysfunctions can result in HM, an important feature of which is excessive proliferation of trophoblasts[31]. Recent study has found that *NLRP7* mutation sped up the differentiation of HM patient-derived hiPSC into trophoblasts[29].

Study demonstrated that when hESCs were exposed to bone morphogenetic protein-4 (BMP4), these cells tended to differentiate into trophoblasts[32]. In addition, hESCs and hiPSCs are maintained with activators of two signaling pathways: the BMP receptor type-1A (BMPR1A) (ALK3) pathway via ACTIVIN and the mitogen-activated protein kinase kinase/ERK signaling pathway via FGF2[33]. For this reason, improved trophoblasts differentiation can be achieved by the addition of ACTIVIN-A/NODAL/TGF-β signaling inhibitor (A83-01) and FGF2 signaling inhibitor (PD173074), in addition to BMP4 (referred to as BAP conditions). So we generated trophoblast cells from hESCs using an established protocol of BAP treatment[29]. During the differentiation of p-hESCs into trophoblasts, we observed that BAP-treated p-hESCs began to express the early trophoblast lineage marker CDX2 On day 2. Notably, p-NLRP7$^{-/-}$ exhibited higher CDX2 levels compared to p-WT cells (Supplementary Fig. 2A, and B). By day 4, the expression of KRT7 followed similar trends to CDX2 (Supplementary Fig. 2B, and C). Meanwhile, we also found higher levels of DNA damage in NLRP7$^{-/-}$ trophoblasts, similar to p-hESCs. Since extraembryonic cells are more tolerant to DNA damage than embryonic cells, we then examined the expression of Active Caspase 3 and found that NLRP7 knockout did not significantly increase the apoptosis level in these cells (Supplementary Fig. 2D). These results suggest that deletion of *NLRP7* accelerate the differentiation of hESCs into trophoblasts, but has no significant effect on the survival of these cells, consistent with previous studies[29,34].

Deletion of *NLRP7* affects the development of blastoids, which is related to the increased levels of DNA damage

NLRP7 knockout caused genetic instability in p-hESCs and also accelerated the differentiation of these cells into trophoblasts. So, does the loss of NLRP7 in early human embryos have a similar phenotype? To test this question, we used blastoids as an in vitro model for blastocysts, both of which have similar molecular and developmental properties. Using the 5i/L/A induced culture system[35] (Fig. 2A), naïve-like cell clones began to appear after 8–10 days, exhibiting a typical "dome-shaped" morphology and expressing the naïve pluripotent stem cell-specific marker KLF17, which was rarely expressed in p-hESCs (Fig. 2B, C). RT-qPCR also confirmed the expression of naïve pluripotent marker in these naïve hESCs (n-hESCs) (Fig. 2D). We then analyzed the DNA damage and apoptosis of n-hESCs, finding markedly increased γH2A.X in n-NLRP7$^{-/-}$ (Fig. 2E, F). Moreover, active caspase 3 staining also revealed elevated apoptosis in n-NLRP7$^{-/-}$ (Fig. 2G, H). Unexpectedly, we found that *NLRP7* knockout affected the long-term culture of n-hESCs in vitro, making n-NLRP7$^{-/-}$ difficult to maintain after passage 20, likely due to accumulated DNA damage (Fig. 2I). These results demonstrated that the knockout of *NLRP7* leads to DNA damage and apoptosis in the n-hESCs, consistent with the observations in p-hESCs.

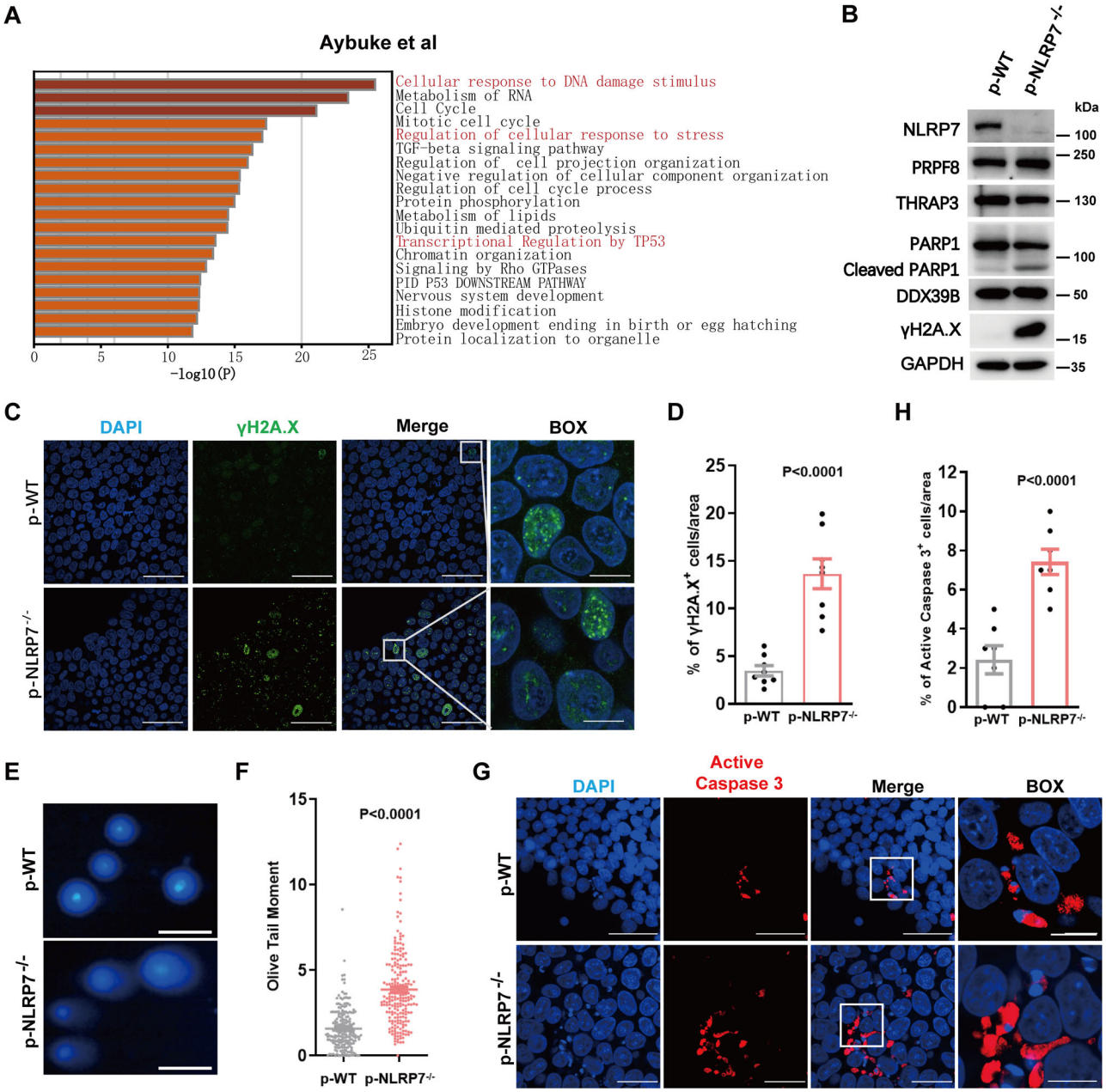

Fig. 1 | NLRP7 is required for the maintenance of genomic DNA integrity in p-hESCs. A KEGG pathway enrichment analysis of genes affected by *NLRP7* mutation in hiPSCs. The RNA-seq data was derived from the study of Alici-Garipcan et al.[29]. **B** Representative western blot analysis of NLRP7, γH2A.X, PARP1, PRPF8, THRAP3 and DDX39B in p-WT and p-NLRP7$^{-/-}$. **C** Representative immunofluorescent images of p-WT and p-NLRP7$^{-/-}$ for the DNA damage marker γH2A.X (green). The nuclei were counterstained with DAPI and are shown in blue. Increased γH2A.X^{+} cells are detected in p-NLRP7$^{-/-}$. Scale bar, 50 μm. BOX, Scale bar, 10 μm. **D** Quantification of the γH2A.X foci in the immunofluorescent staining shown in (**C**). Non-parametric test. **E** Comet assay reveals severe DNA damage in the p-NLRP7$^{-/-}$. Genomic DNA was stained with DAPI and imaged after single-cell electrophoresis. More than 200 cells were analyzed in each group. **F** Quantification for the length of the tail movement. Data are shown as mean ± SEM. $^{**}P < 0.001$, Non-parametric test. **G** Representative immunofluorescent images of p-WT and p-NLRP7$^{-/-}$ for the apoptosis marker active caspase 3 (Red). Scale bar, 50 μm. BOX, Scale bar, 10 μm. **H** Quantification of the Active Caspase 3 in the immunofluorescent staining shown in (**G**). Data are shown as mean ± SEM. Student's *t*-test.

Early embryonic cells are hypersensitive to DNA damage, even a small amount of DNA damage can result in apoptosis in these cells[5]. So, How *NLRP7* loss affect the formation and development of blastoids? According to previously reported induction culture methods[36], we obtained blastocyst-like structures containing inner cell mass (ICM)-like and trophectoderm-like compartments with a visible cavity (Fig. 3A, B). From day 4 onwards, the cell aggregates began to form cave-like structures, and by day 8 or 9, these blastoids reached ~250 μm in diameter (Fig. 3B). *NLRP7* depletion did not significantly affect the size of the formed blastoids (Fig. 3C). Next, we set out to identify the lineage composition of human blastoids through immunofluorescence analysis. We found that the outer cells (trophectoderm-like cells, TLCs) of the blastoids stained positive for trophectoderm marker GATA3, while OCT4 was highly expressed in ICM-like cells (Fig. 3D). However, compared to wild type (WT) blastoids, NLRP7$^{-/-}$ blastoids exhibited relatively small ICM-like structures and fewer OCT4-positive cells (Fig. 3D, E). More importantly, NLRP7$^{-/-}$ blastoids showed higher expression levels of γH2A.X (Fig. 4A, B) and active caspase 3 (Fig. 4C, D), indicating higher levels of DNA damage and apoptosis. These findings are consistent with the results observed in the p-hESCs (Fig. 1C, G) and n-hESCs (Fig. 2E, G). Thus, the smaller ICM-like cells in NLRP7$^{-/-}$

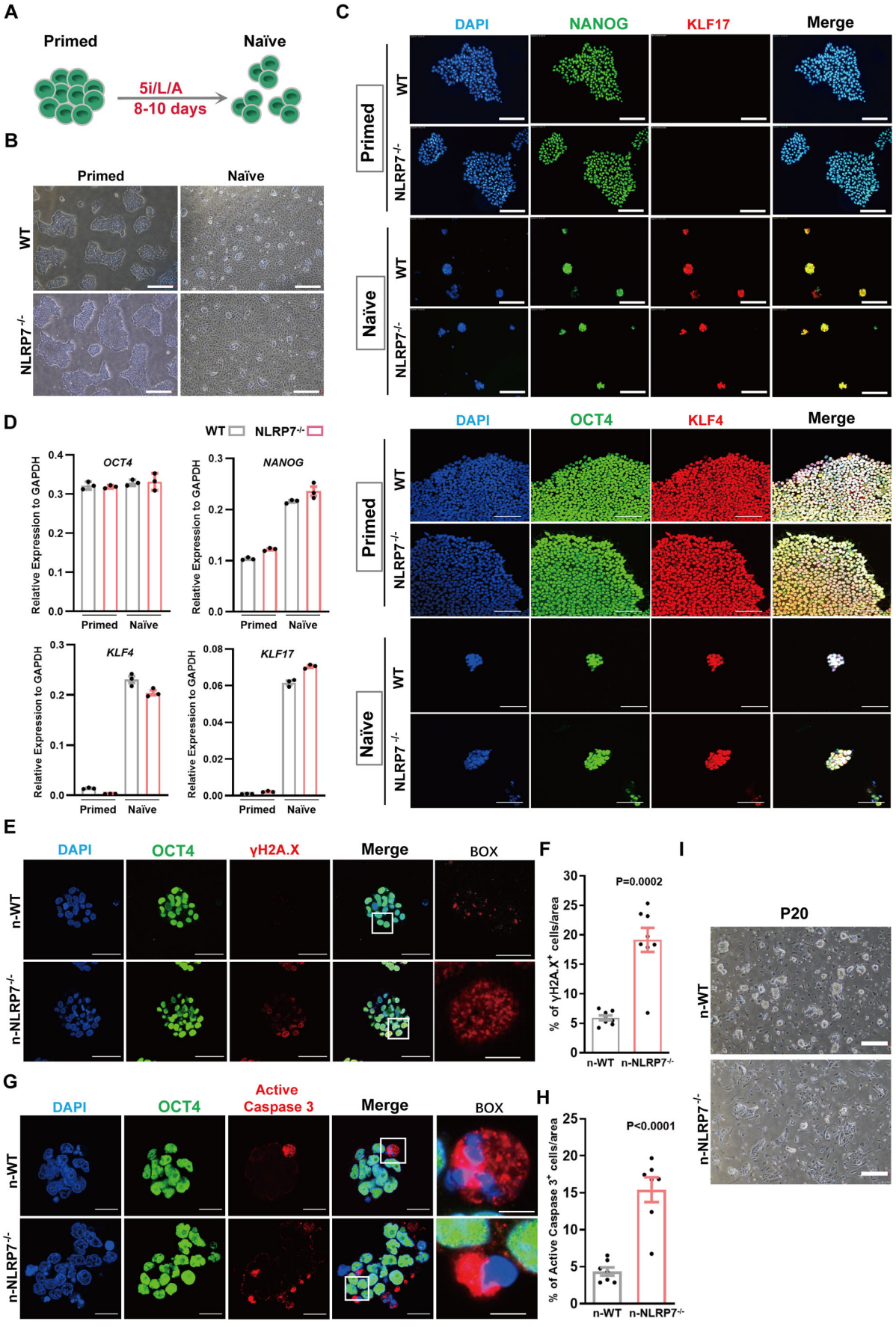
A
Primed
Naïve
5i/L/A
8-10 days
B
Primed
Naïve
WT
NLRP7-/-
C
DAPI
NANOG
KLF17
Merge
Primed
Naïve
WT
NLRP7-/-
D
WT
NLRP7-/-
OCT4
NANOG
KLF4
KLF17
Relative Expression to GAPDH
Primed
Naïve
DAPI
OCT4
KLF4
Merge
E
DAPI
OCT4
γH2A.X
Merge
BOX
n-WT
n-NLRP7-/-
F
P=0.0002
% of γH2A.X+ cells/area
n-WT
n-NLRP7-/-
G
DAPI
OCT4
Active Caspase 3
Merge
BOX
H
P<0.0001
% of Active Caspase 3+ cells/area
I
P20

Fig. 2 | *NLRP7* knockout causes DNA damage and apoptosis in n-hESCs. **A** Schematic of the chemical resetting of p-hESCs to n-hESCs. **B** Representative phase-contrast images of resetting n-hESCs cultures. Scale bars, 100 µm. **C** Immunostaining of general and naïve pluripotency proteins in p-hESCs and established resetting n-hESCs. Scale bars, 100 µm. **D** RT-qPCR analysis of general and naïve pluripotency markers in resetting n-hESCs. Data are shown as mean ± SEM. Student's *t*-test. **E** Representative immunofluorescent images of n-WT and n-NLRP7$^{-/-}$ for the DNA damage marker γH2A.X (red). The nuclei were counterstained with DAPI and are shown in blue. Scale bar, 50 µm. BOX, Scale bar, 5 µm. **F** Quantification of the γH2A.X foci in the immunofluorescent staining in (**E**). Data are shown as mean ± SEM. Student's *t*-test. **G** Representative immunofluorescent images of n-WT and n-NLRP7$^{-/-}$ for the Apoptosis marker active caspase 3 (red). The nuclei were counterstained with DAPI and are shown in blue. Scale bar, 20 µm. BOX, Scale bar, 5 µm. **H** Quantification of the Active Caspase 3 in the immunofluorescent staining in (**G**). Data are shown as mean ± SEM. Student's *t*-test. **I** Representative phase-contrast images of n-WT and n-NLRP7$^{-/-}$ at P20. Scale bars, 100 µm.

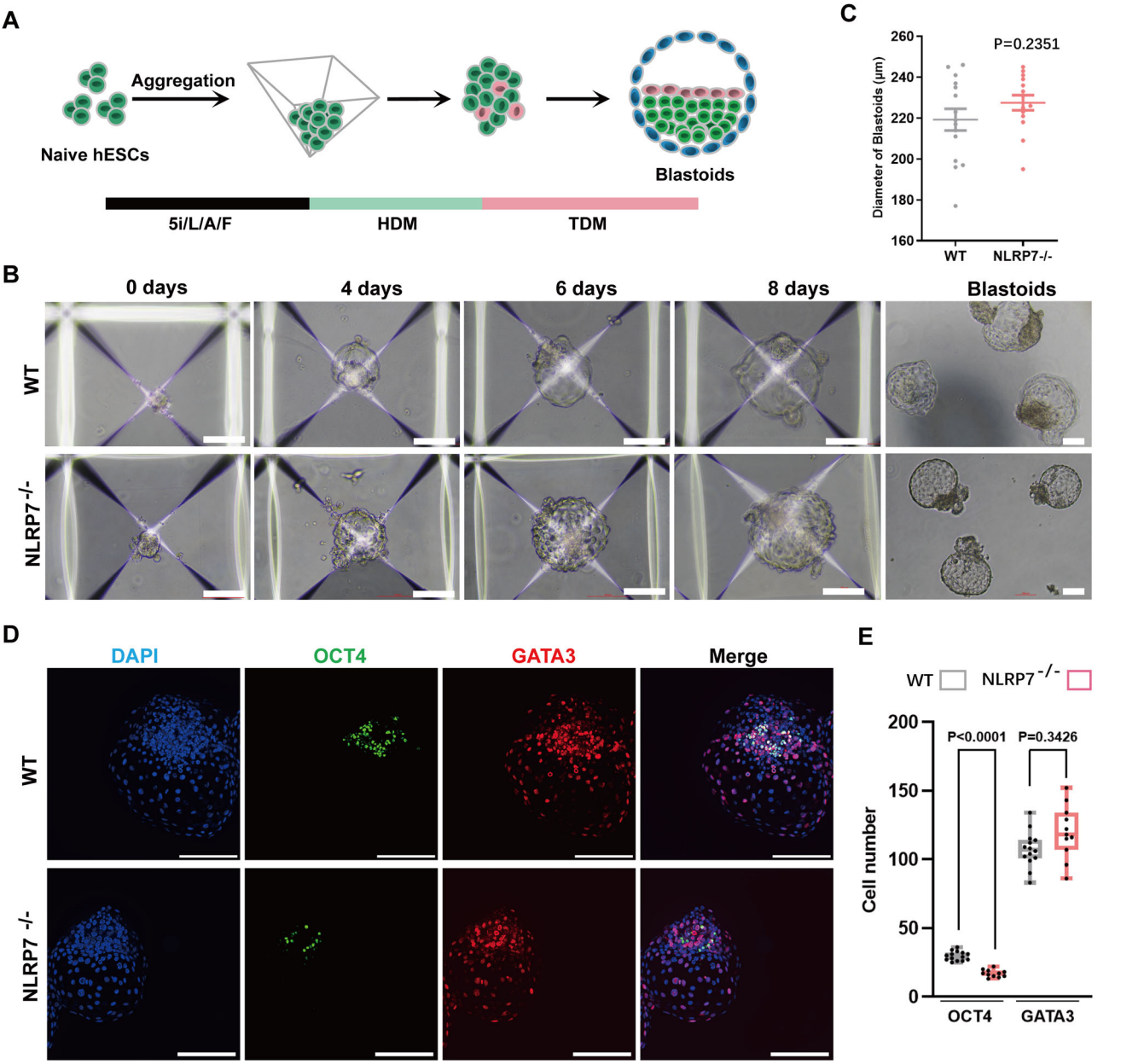

Fig. 3 | *NLRP7* knockout affects human blastoids development. **A** Schematic of human blastoids formation from n-hESCs. Pyramid shape, the microwell of aggrewell 400; Pink cells, primitive endoderm; Green cells, epiblast cells; Naïve embryonic stem cell medium (5i/L/A), Hypoblast differentiation medium (HDM), Trophoblast differentiation medium (TDM). **B** Representative phase-contrast images of cell aggregates at indicated time points during blastoid formation. Scale bar, 100 µm. **C** The diameter of blastoids derived from n-WT and n-NLRP7$^{-/-}$. Data are shown as mean ± SEM. Student's *t*-test. **D** Representative immunofluorescence co-staining images of WT blastoids and NLRP7$^{-/-}$ blastoids for trophectoderm marker GATA3 (red) and the epiblast marker OCT4 (green). Scale bars, 100 µm. **E** Quantification of the number of OCT4^{+} and GATA3^{+} cells in human blastoids (WT Blastoids, $n = 14$ biological replicates; *NLRP7*$^{-/-}$ blastoids, $n = 11$ biological replicates). Box plots show median (center line), 25th and 75th percentiles (bottom and top of the box, respectively), and minimum and maximum values (bottom and top whisker, respectively). Data are shown as mean ± SEM. Student's *t*-test.

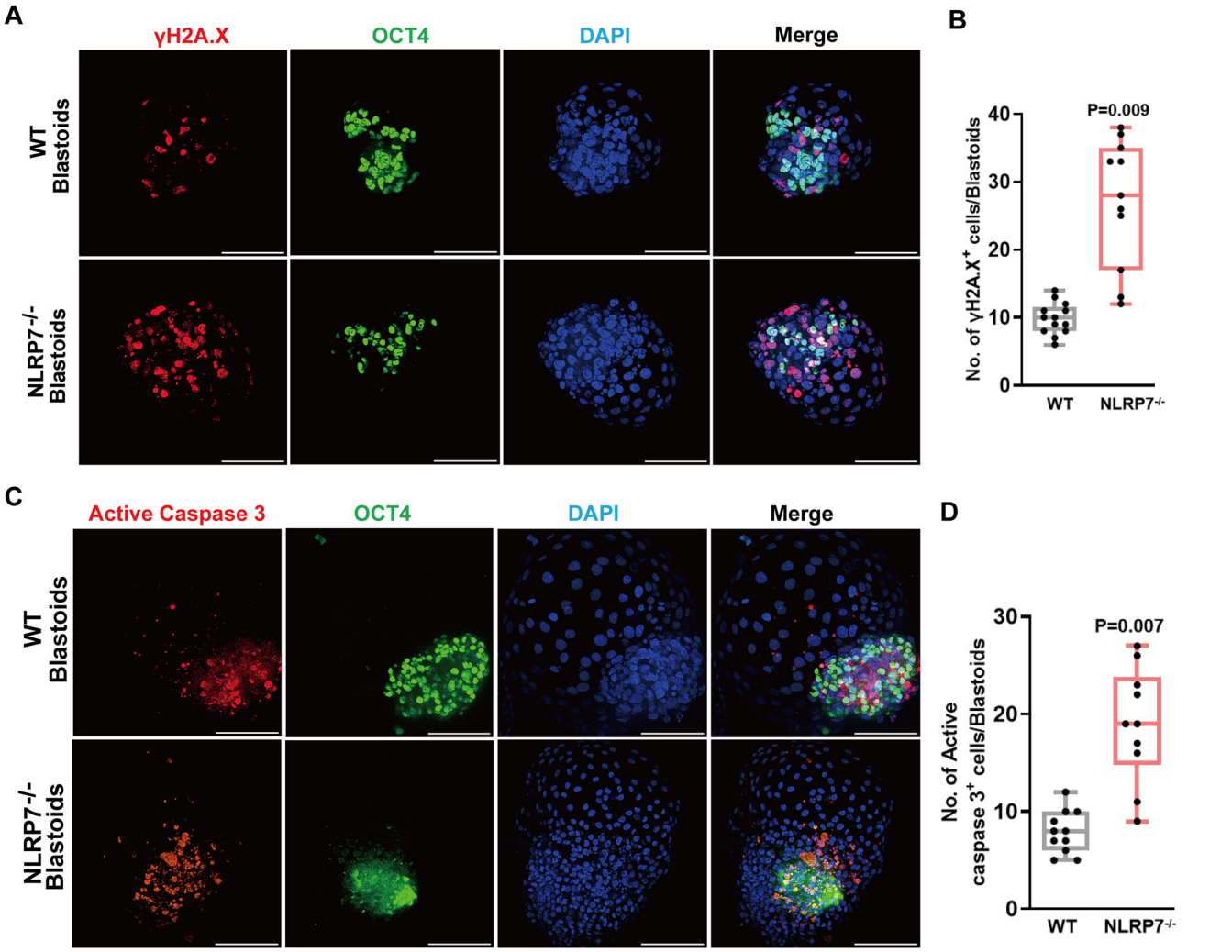

Fig. 4 | *NLRP7* knockout induces apoptosis of embryonic cells in blastoids. **A** Representative immunofluorescent images of wild type and *NLRP7* knockout blastoids at day 3 and day 4 for the DNA damage marker γH2A.X (red) and the epiblast marker OCT4 (green). The nuclei were counterstained with DAPI and are shown in blue. Elevated DNA damage is detected in the $NLRP7^{-/-}$ blastoids, and most of the γH2A.X^{+} cells co-express OCT4. Scale bar, 100 μm. **B** Quantification of the γH2A.X-positive cells in the immunofluorescent staining (WT Blastoids, $n = 13$ biological replicates; $NLRP7^{-/-}$ blastoids, $n = 11$ biological replicates) in (**A**). Box plots show median (center line), 25th and 75th percentiles (bottom and top of the box, respectively), and minimum and maximum values (bottom and top whisker, respectively). Data are shown as mean ± SEM. Student's *t*-test. **C** Representative immunofluorescent images of wild type and *NLRP7* knockout blastoids at day 4 for the Apoptosis marker active caspase 3 (red) and the epiblast marker OCT4 (green). The nuclei were counterstained with DAPI and are shown in blue. Elevated apoptosis is detected in the $NLRP7^{-/-}$ blastoids, and most of the active caspase 3^{+} cells co-express OCT4. Scale bar, 100 μm. **D** Quantification of the active caspase 3^{+} cells in the immunofluorescent staining (WT Blastoids, $n = 11$ biological replicates; $NLRP7^{-/-}$ blastoids, $n = 10$ biological replicates) in (**C**). Box plots show median (center line), 25th and 75th percentiles (bottom and top of the box, respectively), and minimum and maximum values (bottom and top whisker, respectively). Data are shown as mean ± SEM. Student's *t*-test.

blastoids may be associated with increased levels of DNA damage, leading to apoptosis of early embryonic cells. This is in line with the findings in mouse mosaic embryos[37,38].

Because early embryonic cells are highly sensitive to DNA damage, their survival can be significantly affected once a large amount of DNA damage occurs. Therefore, we tested the efficiency of deriving n-hESCs from these blastoids. Using 5i/L/A conditions, we successfully derived n-hESCs from WT and $NLRP7^{-/-}$ blastoids (Supplementary Fig. 2E). However, the efficiency was significantly lower for $NLRP7^{-/-}$ blastoids (Supplementary Fig. 2F). Together, these results demonstrated that NLRP7 dysfunction leads to increased DNA damage and elevated apoptosis levels in early human embryonic cells, ultimately affecting the development and survival of these cells.

NLRP7 interacts with factors related to AS and DDR

To elucidate the molecular mechanism by which NLRP7 dysfunction promotes DNA damage and apoptosis, we constructed a FLAG-tagged NLRP7 overexpression cell line (NLRP7 Overexpression, NLRP7-OE). First, we examined the subcellular localization of NLRP7 in p-hESCs. Under normal circumstances, NLRP7 was mainly located in the cytoplasm (Fig. 5A), consistent with previous reports[18,39]. Notably, the localization of NLRP7 did not also change significantly even after treatment with the DNA damage inducing agents Etoposide (Etop) and Hydroxyurea (HU). However, NLRP7 hardly co-localized with DNA damage marker γH2A.X under either condition, contrary to Rad51 (Fig. 5A). These findings suggest that NLRP7 is not directly involved in DNA damage repair. Given its primary cytoplasmic location, NLRP7 may regulate the expression of other genes or the localization of proteins to maintain the genetic stability of early human embryonic cells.

To further investigate the role of NLRP7 in DDR in hESCs and early human embryonic development, we performed immunoprecipitation-mass spectra (IP-MS) with NLRP7-OE and identified 190 proteins that interacted with NLRP7 protein (Fig. 5B, E). KEGG analysis demonstrated that NLRP7

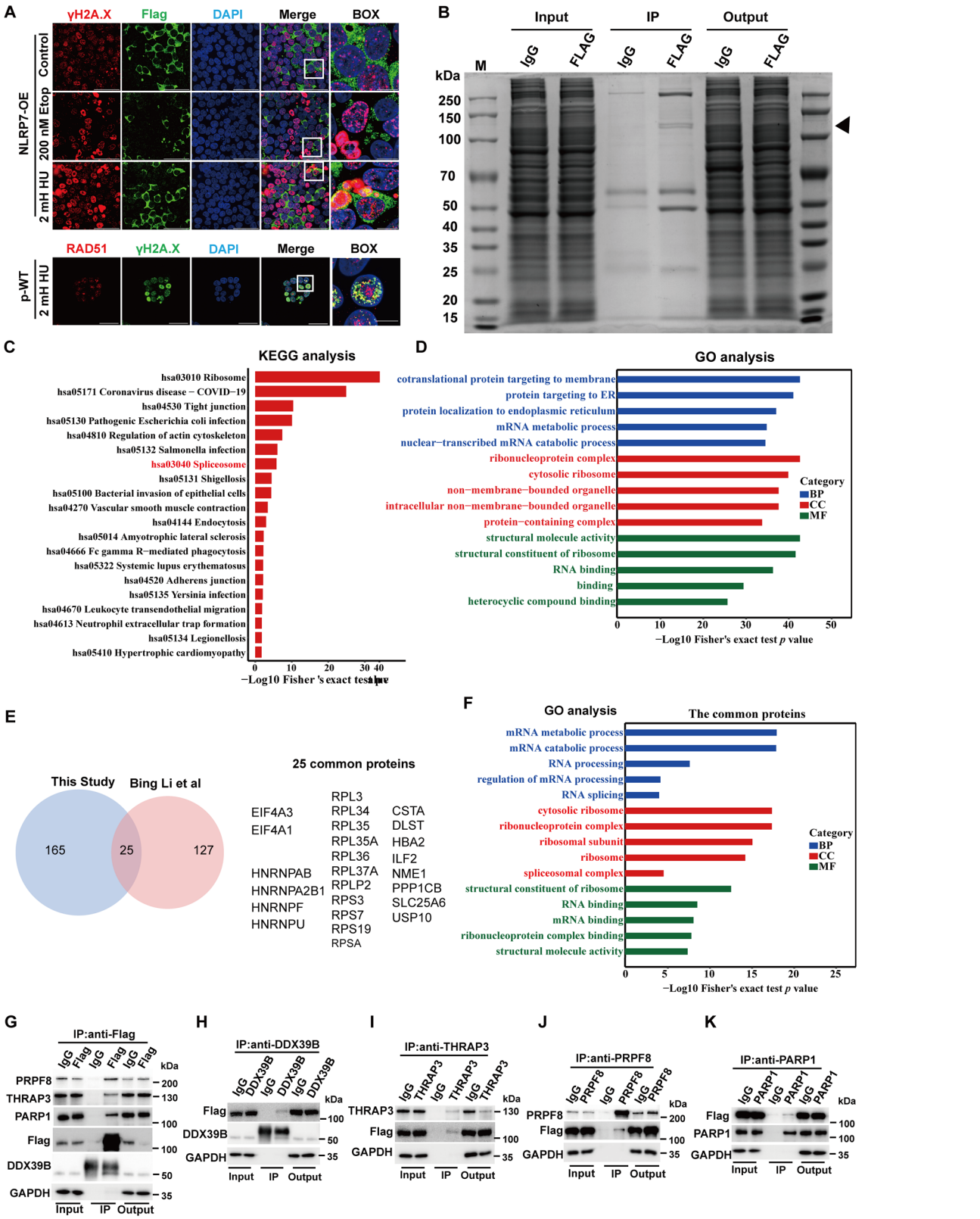

Fig. 5 | NLRP7 regulates alternative splicing in p-hESCs. A Localization of NLRP7, RAD51, and DNA damage marker γH2A.X under different conditions. Scale bar, 50 μm. BOX, Scale bar, 10 μm. **B** Representative image of silver staining for proteins immunoprecipitated with NLRP7 using an anti-Flag antibody. The Flag-NLRP7 band is indicated with a black triangle. **C** KEGG analysis for proteins interacting with NLRP7 showed enriched Microbial infection and spliceosome-associated terms. **D** GO analysis for proteins interacting with NLRP7 showed enriched RNA processing-associated terms. **E** Left: Venn diagram showed overlap between the proteins that interacted with NLRP7 from this study and another independent study[39]. Right: List of proteins in common is given. **F** GO analysis for proteins in common showed enriched RNA processing and RNA splicing associated terms. **G–K** Co-IP revealed the interaction of NLRP7 with factors related to AS and DDR, including DDX39B, PRPF8, THRAP3, and PARP1.

interacting proteins were enriched into biological processes related to COVID-19 infection, bacterial invasion, and immunity, which was consistent with NLRP7's known role in immunomodulation. Unexpectedly, we found that NRLP7 is involved in the formation of spliceosomes (Fig. 5C). Moreover, Gene Ontology (GO) term analysis revealed that many NLRP7-interacting proteins were enriched in RNA processing-related processes, particularly in "RNA splicing", indicating that NLRP7 plays a role in regulating mRNA alternative splicing (Fig. 5D). Recent study has shown that NLRP7 interacted with ubiquitin-specific protease10 (USP10), which catalyzed its deubiquitination in colorectal cancer (CRC)[39]. KEGG and GO analysis of Co-immunoprecipitation (Co-IP) data from this study revealed that NLRP7 was also involved in immunity and RNA splicing (Supplementary Fig. 3A, 3B). By comparing our Co-IP data with those from Bing Li et al.[39], we identified 25 common interacting proteins, including USP10 (Fig. 5E). KEGG and GO analysis of these shared proteins further confirmed their involvement in RNA splicing, supporting the reliability of our findings (Fig. 5F and Supplementary Fig. 3C).

Considering that NLRP7 is involved in the regulation of RNA splicing, and its dysfunctions led to the genetic instability of early human embryonic cells, we then analyzed the interaction between NLRP7 and splice-related proteins involved in DNA damage repair. Among the 190 interacting proteins, we identified some factors related to both AS and DDR, such as DDX39B[40], PRPF8[41], and THRAP3[42] (Fig. 5G–J). Notably, we also detected an interaction of NLRP7 with PARP1, a key protein in DNA damage repair[43], indicating that NLRP7 is involved in the DDR of hESCs (Fig. 5K). Although NLRP7 could interact with these proteins, NLRP7 deletion did not affect their localization (Supplementary Fig. 4A), nor did it significantly change their expression (Fig. 1B, Supplementary Fig. 4B), except for upregulation of Cleaved PARP1 (Fig. 1B), which may be associated with elevated levels of DNA damage after NLRP7 loss. Taken together, these results suggested that NLRP7 might not directly participate in DDR, but instead indirectly affected DNA damage repair by regulating RNA splicing through interactions with other factors.

NLRP7 regulates alternative splicing of HR-related genes

Given NLRP7's involvement in RNA splicing, we then performed RNA sequencing on p-WT and p-NLRP7$^{-/-}$ to analyze altered splicing events. NLRP7 deletion resulted in changes in the expression of more than 700 genes (Supplementary Fig. 3D). Gene Ontology (GO) analysis revealed that NLRP7 knockout led to significant changes in apoptosis, female pregnancy, and a lot of biological processes involved in immune regulation, consistent with what NLRP7 is known to do (Fig. 6A). Subsequently, we performed an alternative splicing analysis. 1162 alternative splicing events were identified with at least a 10% change in percent spliced in (PSI) (Fig. 6B). GO analysis revealed that some of these alternatively spliced genes were enriched in the "HR signaling pathway" (Fig. 6C). We also confirmed the aberrant splicing of key genes in the pathway, such as *RAD51* and *BRCA1*[44], through visualization using Sashimi plots (Fig. 6D, E). These findings were further validated via RT-qPCR assays (Fig. 6F). Our results demonstrate that NLRP7 is involved in maintaining genetic stability by regulating the AS of HR-related genes.

In summary, our findings identified NLRP7 as a crucial regulator linking DNA damage, alternative splicing, and early human embryonic development. NLRP7 dysfunctions alter the splicing of key HR-related genes, such as *RAD51* and *BRCA1*, impairing the DNA damage repair process, and ultimately lead to early embryonic development failure.

Discussion

Early embryonic development failure is mainly associated with chromosomal abnormalities[2,30]. *NLRP7* mutations can lead to recurrent miscarriage or HM[21]. In this study, we first demonstrated that NLRP7 regulates early human embryogenesis by maintaining genetic stability. Deletion of *NLRP7* resulted in increased DNA damage in both hESCs and blastoids, leading to heightened susceptibility of embryonic cells in blastoids to apoptosis, and consequently fewer ICM-like cells. In addition, the difficulty of maintaining long-term stable passage of n-NLRP7$^{-/-}$ in vitro and the reduced efficiency of deriving n-hESCs from NLRP7$^{-/-}$ blastoids might also be attributed to the elevated levels of DNA damage. This may be related to the expression pattern of *NLRP7*, which decreased gradually from oocyte to embryo on day 3 after fertilization but increased significantly by day 5[20]. This expression pattern corresponds to the embryonic genome activation (EGA) and blastocyst development stage[45]. A recent study has shown that *NLRP7* mutations affect the oocyte quality and cause embryo development arrest. In addition, this study confirmed that NLRP7 interacts with maternal factors, such as KHDC3L[46], consistent with previous findings[18]. In fact, *KHDC3L* mutations have also been associated with embryo development arrest[47] and HM[18]. Our previous study has shown that KHDC3L is involved in maintaining the genetic stability in early human embryonic cells, and its dysfunction resulted in DNA damage and impaired early embryonic development[48]. Therefore, it is not difficult to understand that NLRP7 plays a crucial role in maintaining genetic stability in early human embryonic cells.

AS is a versatile mechanism to increase the complexity and diversity of the mammalian transcriptome[49]. Recent studies have reported that AS is associated with genetic stability[50] and early embryonic development[51]. Deletion or dysfunction of AS-related factors can cause DNA damage, which in turn affects embryonic development[52]. When exploring the molecular mechanism by which NLRP7 defects lead to elevated DNA damage levels, we found that NLRP7 could not only interact with factors associated with AS and DDR, including DDX39B, PRPF8, and THRAP3 but also with PARP1. Beyond its role in DNA damage repair, PARP1 can also bind to RNA and splicing factors to regulate AS[53]. Therefore, these results suggest that NLRP7 regulates early human embryonic development by mediating RNA splicing. Furthermore, we discovered that NLRP7 modulates DDR by influencing the expression of HR-related genes, such as *RAD51* and *BRCA1*. Aberrant splicing of these genes would result in DNA damage accumulation and subsequent apoptosis. However, whether NLRP7 directly interacts with RNA and functions as an AS factor remains to be investigated.

In summary, we have firstly demonstrated that NLRP7 plays a crucial role in maintaining genetic stability by regulating the AS of HR-related genes. The altered splicing of these genes may impair DNA damage repair, leading to damage accumulation and inducing apoptosis in both hESCs and blastoids, and ultimately resulting in the developmental failure of early human embryos.

Methods

Ethics statement

All human ESCs and blastoid experiments were performed at the Center of Tissue Engineering and Stem Cells of Guizhou Medical University and followed the 2016 and 2021 Guidelines released by the International Society for Stem Cell Research (ISSCR). Human ESCs and blastoids work was reviewed and approved by the Ethics Committee of Guizhou Medical University. This work did not exceed a developmental stage normally associated with 14 consecutive days in the culture of blastoids as far as human embryo models are concerned.

Cell lines

The H9 hESCs were provided by Dr. Tianqing Li from Kunming University of Science and Technology. All cell culture experiments involving hESCs were approved by the Stem Cell Oversight Committee at the Guizhou Medical University and carried out in accordance with the approved guidelines. The 293T cells used in this study were purchased from the cell bank of Kunming Institute of Zoology, Chinese Academy of Sciences. The mouse embryonic fibroblasts (MEFs) were purchased from Millipore (PMEF-CFL).

p-hESCs culture and differentiation

p-hESCs were maintained on 1:30 diluted hESC-qualified Matrigel (Corning, 354277) with DMEM/F-12 (Gibco, C11330500CP) coated plates and cultured in mTeSR1 medium (STEMCELL Technologies) in a humidified

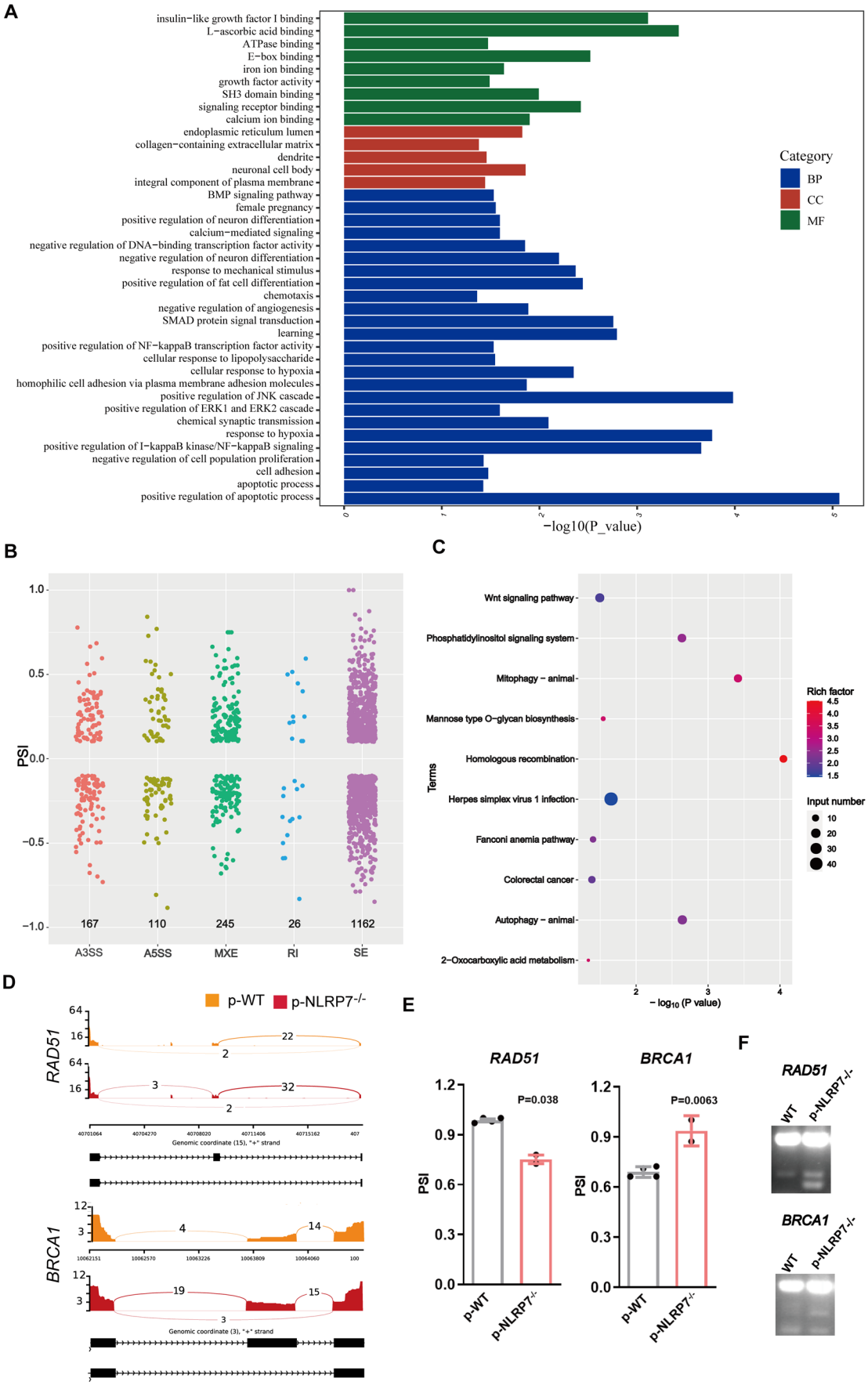
A
insulin−like growth factor I binding
L−ascorbic acid binding
ATPase binding
E−box binding
iron ion binding
growth factor activity
SH3 domain binding
signaling receptor binding
calcium ion binding
endoplasmic reticulum lumen
collagen−containing extracellular matrix
dendrite
neuronal cell body
integral component of plasma membrane
BMP signaling pathway
female pregnancy
positive regulation of neuron differentiation
calcium−mediated signaling
negative regulation of DNA−binding transcription factor activity
negative regulation of neuron differentiation
response to mechanical stimulus
positive regulation of fat cell differentiation
chemotaxis
negative regulation of angiogenesis
SMAD protein signal transduction
learning
positive regulation of NF−kappaB transcription factor activity
cellular response to lipopolysaccharide
cellular response to hypoxia
homophilic cell adhesion via plasma membrane adhesion molecules
positive regulation of JNK cascade
positive regulation of ERK1 and ERK2 cascade
chemical synaptic transmission
response to hypoxia
positive regulation of I−kappaB kinase/NF−kappaB signaling
negative regulation of cell population proliferation
cell adhesion
apoptotic process
positive regulation of apoptotic process
Category
BP
CC
MF
−log10(P_value)
B
PSI
1.0
0.5
0.0
−0.5
−1.0
167
110
245
26
1162
A3SS
A5SS
MXE
RI
SE
C
Wnt signaling pathway
Phosphatidylinositol signaling system
Mitophagy − animal
Mannose type O−glycan biosynthesis
Homologous recombination
Herpes simplex virus 1 infection
Fanconi anemia pathway
Colorectal cancer
Autophagy − animal
2−Oxocarboxylic acid metabolism
Terms
− log10 (P value)
Rich factor
Input number
D
p-WT
p-NLRP7−/−
RAD51
BRCA1
Genomic coordinate (15), "+" strand
Genomic coordinate (3), "+" strand
E
RAD51
BRCA1
P=0.038
P=0.0063
PSI
p-WT
p-NLRP7−/−
F
RAD51
BRCA1
WT
p-NLRP7−/−

Fig. 6 | NLRP7 is required for the RNA splicing of genes involved in homologous recombination. **A** GO enrichment analysis showing biological processes (BPs), cellular components (CCs), and molecular functions (MFs) affected by NLRP7 loss in hESCs. **B** The number of changed alternatively spliced events after *NLRP7* knockout in p-hESCs. We placed splicing events into groups according to rMATS: (1) alternative 3′SS (A3SS), (2) alternative 5′SS (A5SS), (3) mutually exclusive exons (MXE), (4) retained intron (RI), and (5) skipped exon (SE). The cumulative number of events in each cell group with an inclusion level difference (ILD) > 0.1 or <−0.1 and a false discovery rate (FDR) < 0.05 are shown. **C** KEGG pathway enrichment analysis of all genes whose AS were affected by *NLRP7* knockout in p-hESCs. The number of genes indicated by circle sizes and adjusted *p* values indicated by red to blue colors. **D** Representative Sashimi plot showing the increased SEs of the *RAD51* and *BRCA1* genes in p-NLRP7$^{-/-}$ compared with p-WT. **E** Calculated PSI value of the alternatively spliced genes associated with HR in both p-WT and p-NLRP7$^{-/-}$. Data are shown as mean ± SEM. Student's *t*-test. **F** RT-qPCR confirms the altered splicing of HR-associated genes in (**E**).

incubator under 5% CO2 at 37 °C. Cells were regularly passaged when they reached 80–90% confluency with TrypLE Express (Gibco, 12605010), usually 3–4 days at a ratio of 1:8–1:10. When passaged, the p-hESCs were washed by PBS twice, then followed by digesting with TrypLE Express for 5 min to dissociate the clones into single cells. Cells were seeded onto Matrigel-coated surfaces in mTeSR1 supplemented with 10 mM Y-27632 (SELLECK, S1049). For regular maintenance, cells were cultured in 35 mm cell culture dishes, and the medium was changed every day.

For trophoblast differentiation, the day after passaging onto Matrigel-coated dishes at 1.2×10^4 cells/cm^2, the culture medium was changed to DMEM/F12 medium (Gibco, C11330500CP) with KnockOut SR (Gibco, 10828010) that had been conditioned by MEFs and supplemented with 10 ng/ml FGF2. On the next day, the medium was changed to 10 ng/ml BMP4 (Peprotech, 120-05), 1 μM A83-01 (SELLECK, S7692), and the 0.1 μM PD173074 (SELLECK, S1264) containing (BAP) DMEM/F12/KOSR medium not conditioned with MEF feeder cells. Control cultures were maintained in a conditioned medium containing 10 ng/ml FGF2.

Culture of naïve hESCs (n-hESCs)

n-hESCs were converted from the corresponding p-hESCs. n-hESCs were cultured in 5i/L/A medium containing 1:1 of DMEM/F-12 and Neurobasal (Gibco, 21103049), 1% N2 supplement (Gibco,17502048), 2% B27 supplement (Gibco, 17504044), 0.5% KnockOut SR, 1 mM GlutaMAX (Gibco, 35050061), 1% MEM non-essential amino acids (Gibco, 11140050), 1% penicillinstreptomycin (Gibco, 10378016), 0.1 mM 2-mercaptoethanol (Sigma, M3148), 50 μg/ml bovine serum albumin (BSA, Sigma, B2064), and the following small molecules and cytokines: 1 μM PD0325901 (Selleck, S1036), 1 μM CHIR99021 (Selleck, S2924), 0.5 μM SB590885 (Selleck, S2220), 1 μM WH-4-023 (Selleck, S7565), 10 μM Y-27632 (Selleck, S1049), 20 ng/ml recombinant human LIF (Peprotech, 300-05), 20 ng/ml Activin A (Peprotech, 120-14 P), 8 ng/ml FGF2 (Millipore, GF003). n-hESCs were cultured on Mitomycin C (Sigma, M0503) inactivated mouse embryonic fibroblasts (MEFs) feeders with daily refreshed medium under 20% O_2 and 5% CO_2 at 37 °C and passaged with TryPLE express. n-hESCs were passaged every 4–5 days at a ratio of 1:6.

Culture of 293T cells

293T cells were cultured in DMEM medium [DMEM (Gibco) supplemented with 10% FBS (Gibco), 1X GlutaMAX (Gibco), and 1% penicillin–streptomycin (Gibco)]. When confluency reached 80–90%, cell medium was aspirated and 1 ml 0.1% trypsin–EDTA was added to each well of six-well plates. Due to the poor adherence of 293T cells, they easily fall off from the bottom of the surfaces. Therefore, in order to increase its adherent ability, cell culture plates could be coated with 0.1% gelatin for 30 min at room temperature. 293T cells were passaged every 3 days at a ratio of 1 : 6–1 : 9.

Generation of human blastoids in AggreWell

Because the quality of n-hESCs is crucial for the formation of Blastoids. Therefore, we performed an in vitro induction culture of blastoids using stable n-hESCs at an early passage (no more than 20 passages). For the generation of human blastoids, 70–80% confluent n- hESCs were dissociated into single cells by incubation with TrypLE Express at 37 °C for 5 min. Cells were collected and resuspended in 5i/L/A medium after centrifugation at 200×*g* for 3 min. After centrifugation, the cell pellet was resuspended in 5i/L/A medium and then transferred onto the gelatin-coated plate and incubated at 37 °C for one hour to remove MEFs. After feeder cell adhesion, The supernatant containing n-hESCs was collected and passed through a 40 μm cell strainer, and the cell number was determined using Trypan Blue staining to assess cell viability. Approximately 3×10^4 cells (around 25 cells per microwell) were resuspended in 1 ml of 5i/L/A medium and seeded into one well of an AggreWell 400 24-well plate (Stemcell, 34411) pretreated with anti-adherence rinsing solution (Stem Cell Technologies, 07010) according to the instructions, and then cultured under 20% O_2 and 5% CO_2 at 37 °C. Aggregates formed the other day, and the medium was replaced every day. Usually, spontaneous cavitation took place gradually from day 3.

Derivation of n-hESCs from human blastoids

The previously described protocols to derive and culture n-hESCs and human TSCs were used[36]. In brief, individual human blastoids were transferred onto MEFs and cultured in a 5i/L/A medium. Within 4–5 days, outgrowths could be observed. Outgrowths were dissociated with TrypLE Express and passaged onto newly prepared MEF plates. Individual colonies were manually picked, dissociated, and cultured in their corresponding media.

Generation of stable cell lines

The lentivirus technology was used for the expression of specific genes. In brief, HEK293T cells were transfected by means of Lipofectamine 2000 (Invitrogen) with pSPAX2, pMD2.G, and p-TOMO containing human *NLRP7* CDS. Viral supernatants were collected 72 h after transfection and were concentrated using ultrafiltration membranes (Millipore, UFC9100). Then, p-hESCs were infected with a concentrated virus in the presence of polybrene (10 μg/ml). About 2–3 weeks, Single-cell clones of p-hESCs that had been stably transfected with p-TOMO expressing NLRP7 were picked manually.

Plasmid construction

Cas9 expression plasmid pSpCas9(BB)-2A-Puro (PX459) V2.0 (#62988) was purchased from Addgene, Inc. The design (http://tools.genome-engineering.org) and construction of sgRNAs were performed according to previous experimental methods. The brief process is as follows: To knock out the *NLRP7* gene in p-hESCs, we designed two sgRNAs specifically targeting the second exon of the gene, sgRNA1 (TTCTGTAGCACGTCTTCGA) and sgRNA2 (TGCAGAGTCCACTCTAGCT). Then, these sgRNAs were ligated into the Cas9 expression plasmid pSpCas9(BB)-2A-Puro (PX459) V2.0, respectively, and validated using Sanger sequencing.

Transfection and antibiotic selection

The sgRNAs and Cas9 co-expression plasmid pSpCas9(BB)-2A-Puro (PX459) V2.0 were introduced into p-hESCs using Lipofectamine™ Stem Reagent. The specific process is carried out according to the instruction manual. Briefly, 30–40% confluent p-hESCs in a 35 mm cell culture dish were transfected by using Lipofectamine™ Stem Reagent mixed with 2 μg plasmids (pSpCas9(BB)-2A-Puro (PX459) V2.0) which contain targeted sgRNAs. In order to improve cell survival efficiency, Prior to transfection, pre-treat the p-hESCs cultures with ROCK inhibitor Y-27632 at a final concentration of 10 μM in mTeSR1 for 2–6 h. 3–4 days after transfection, the cells could be screened for 3–5 days by 1 μg/ml puromycin. About 2–3 days after Puromycin was removed, the cells were digested for passage when the confluency reached 70–80%.

Screening of gene knockout cells

For passage of Puromycin screened cells, the cell density was adjusted to 5×10^4/ml using medium after digested into single cells by using TrypLE Express or Trypsin–EDTA, and then 2 ml of fresh medium was added to a 35-mm cell culture dish, followed by 10 μl of cell suspension (500 cells). In order to improve cell survival, Rock inhibitor Y-27632 was added to a final concentration of 10 μM. After 24 h, the cells were carefully observed under a microscope to ensure that individual cells were scattered and kept at a sufficient distance from each other. If two cells were gathered together, one of them were removed with 10 μl pipettes. After about 10–14 days, the single cells could grow into clones. Then, some of the cells in these clones could be harvested for PCR and Sanger sequence, and the remaining cells could be used for passage and subsequent expansion experiments.

Genotyping PCR

Clone clumps were directly added into 20 μl PCR mixture. After PCR, loading 5 μl of PCR products into the wells of a 1.5% (wt/vol) agarose gel, and run the gel at 120 V for 30 min. Staining the gel with ethidium bromide (EB) solution for 3–5 min, and then visualizing the DNA band by using the BIO-RAD GelDoc XR, and finally confirming single-band amplifications of PCR fragments based on the predicted size. Primer sequences are listed in Supplementary Table 1.

RT-qPCR analysis

Total RNAs were extracted using the RNAsimple Total RNA Kit (TIANGEN, 4992858). cDNA was synthesized using PrimeScriptRT reagent Kit (Takara, RR037A), and then amplified with SYBR green master mix (Takara, RR820B) by specific primers. GAPDH was used as an internal control, and signals in each sample were normalized against it. Primer sequences are listed in Supplementary Table 1.

Immunoblotting

Cells were lysed with RIPA lysis buffer (Beyotime, P0013B) with proteinase inhibitor cocktail (Beyotime, P1010) and Phosphatase inhibitor cocktail (Beyotime, P1086) for 20 min in ice and centrifuged at 10,000×*g* at 4 °C for 10 min. Supernatants were collected and mixed with 5×SDS–PAGE loading buffer (250 mM Tris–Hcl [pH 6.8], 10% SDS, 0.5% BPB, 50% glycerinum, 5% β-mercaptoethanol) and heated to 100 °C for 10 min. After electrophoresis, protein samples were transferred to the PVDF membrane, which was blocked with a blocking reagent (Roche, 11096176001) for 60 min followed by incubation with primary antibodies and second antibodies, respectively. Images were captured using a Protein Simple FluorChem system. Each experiment was carried out in triplicate, and a representative blot is shown unless otherwise stated.

Immunoprecipitation

p-hESCs (1×10^7 cells) were harvested and lysed in 500 μL mild RIPA lysis buffer (Beyotime, P0013D) with a proteinase inhibitor cocktail for 1 h on ice. After centrifuging at 10,000×*g* at 4 °C for 10 min, The cell lysates were preclear with Protein A/G Magnetic Beads (Thermo Fisher Scientific, 10015D) at 4 °C for 2 h, then the supernatants were collected and incubated with the same Protein A/G Magnetic Beads and primary antibodies at 4 °C overnight according to the manufacturers' protocol. After immunoprecipitation, proteins were fractionated by SDS–PAGE gel followed by immunoblotting analysis. The primary antibodies used were the following: GAPDH (Proteintech, 60004-1-Ig), PRPF8 (Proteintech, 11171-1-AP), THRAP3 (Proteintech, 19744-1-AP), DDX39B (Proteintech, 14798-1-AP), and PARP1 (Proteintech, 13371-1-AP).

Mass spectrometry analysis

Similar to the IP assay, cellular protein extracts from hESCs (H9) were incubated with anti-Flag-NLRP7 followed by protein A/G magnetic beads. Recovered proteins associated with Flag-NLRP7 or IgG were resolved by gel electrophoresis. The bands specifically bound to Flag-NLRP7 were excised, and proteomics screening was accomplished by mass spectrometry analysis on a MALDI-TOF-MS instrument (Bruker Daltonics). The mass spectrometry proteomics data have been deposited to the ProteomeXchange Consortium via the PRIDE partner repository with the dataset identifier PXD059649.

Immunofluorescent staining

Cells are cultured on coverslips until approximately 70–80% confluency. After fixing with 4% (w/v) paraformaldehyde (PFA) for 15 min at room temperature (2 h for blastoids), samples (including: two-dimensional-cultured cells, human blastoids) were permeabilized for 10 min (2 h for blastoids) with 0.2% TritonX-100 in PBS and blocked for 60 min or overnight at 4 °C with 1% bovine serum albumin (BSA). Primary antibodies diluted in blocking buffer were applied to samples and incubated overnight at 4 °C. Samples were washed three times with PBS containing 0.1% Tween-20 (PBS-T), followed by incubation with fluorescently conjugated secondary antibodies diluted in a blocking buffer for 2 h at room temperature. Samples were washed three times with PBS-T. Finally, cells were counterstained with 300 nM 4′,6-diamidino-2-phenylindole (DAPI) solution at room temperature for 10 min. Images were then captured using Nikon-AXR confocal microscope. The primary antibodies and appropriate fluorohore-conjugated secondary antibodies used in this study are as follows: OCT4 (Santa Cruz, sc-5279), NANOG (Thermo Fisher Scientific, PA1-097X), NLRP7 (Abcam, ab105405), KLF17 (ATLAS ANTIBODIES, HPA024629), CDX2 (Abcam, ab76541), GATA3 (Abcam, ab199428), KRT7 (Abcam, ab68459), HLA-G (Santa Cruz, sc-21799), BrdU (BD Biosciences, 347580), γH2A.X (Cell Signaling Technology, 9718S), γH2A.X (abmart, M63324), Active-Caspase 3 (Cell Signaling Technology, 9661S), Rad51 (Abcam, ab133534), Flag (Proteintech, 66008-4-Ig), Flag (abmart, M20008S), DDX39B (Proteintech, 14798-1-AP), THRAP3 (Proteintech, 19744-1-AP), PRPF8 (Proteintech, 11171-1-AP), PARP1 (Proteintech, 66520-1-Ig), GAPDH (Proteintech, 60004-1-Ig), Goat anti-Mouse IgG (H + L) (Thermo Fisher Scientific, A-11001), and Goat anti-Rabbit IgG (H + L) (Thermo Fisher Scientific, A-11012).

Neutral comet assay

Briefly, glass slides were dipped into melted 0.8% agarose for 5 s and air dried. Single P-hESCs were resuspended in ice-cold PBS (Ca^{2+} and Mg^{2+} free) in a concentration of 1×10^6 cells/mL. Cells (10 μL) were added into 70 μL 0.8% melted low-melting-point (LMP, Sangon Biotech, A600015-0025) agarose kept at 37 °C. The cell-agarose suspension was immediately pipetted and evenly spread on the prepared slides, covered by a coverslip. Slides were then kept at 4 °C for 10 min and immersed in neutral lysis solution (2.5 M NaCl, 100 mM Na2EDTA, 10 mM Tris, 1% N-lauroylsarcosine, 1% TritonX-100 [pH 9.5]) for 60 min at room temperature without a coverslip. Slides were washed and incubated in cold neutral electrophoresis buffer (300 mM sodium acetate, 100 mM Tris [pH 8.3]) for 30 min. Electrophoresis was carried out at 1 V/cm, 80 mA for 30 min.

After electrophoresis, the slides were washed, fixed with anhydrous ethanol, and air-dried. DNA was stained with 1 μg/mL DAPI (Invitrogen, D1306) for 30 min at room temperature. After washing with water three times, images were immediately analyzed using a Leica digital camera. Comets were analyzed by image J. A total of 200 cells were counted per slide.

RNA-sequencing analysis

Total RNAs were extracted from hESCs using TRIzol Reagent (Invitrogen, cat. no. 15596026) according to the manufacturer's protocol. DNA digestion was carried out after RNA extraction by DNaseI. RNA quality was determined by examining A260/A280 with NanodropTM One Cspectrophotometer (Thermo Fisher Scientific). RNA Integrity was confirmed by 1.5% agarose gel electrophoresis. Qualified RNAs were finally quantified by Qubit3.0 with a QubitTM RNA Broad Range Assay kit (Life Technologies, Q10210).

2 μg total RNAs were used for stranded RNA sequencing library preparation using KC-DigitalTM Stranded mRNA Library Prep Kit for Illumina® (Catalog no. DR08502, Wuhan Seqhealth Co., Ltd. China) following

the manufacturer's instruction. The kit eliminates duplication bias in PCR and sequencing steps by using a unique molecular identifier (UMI) of 8 random bases to label the pre-amplified cDNA molecules. The library products corresponding to 200–500 bps were enriched, quantified, and finally sequenced on DNBSEQ-T7 sequencer (MGI Tech Co., Ltd. China) with PE150 model.

Raw sequencing data was first filtered by Trimmomatic (version 0.36), low-quality reads were discarded, and the reads contaminated with adaptor sequences were trimmed. Clean Reads were further treated with in-house scripts to eliminate duplication bias introduced in library preparation and sequencing. In brief, clean reads were first clustered according to the UMI sequences, in which reads with the same UMI sequence were grouped into the same cluster. Reads in the same cluster were compared to each other by pairwise alignment, and then reads with sequence identity over 95% were extracted to a new sub-cluster. After all sub-clusters were generated, multiple sequence alignment was performed to get one consensus sequence for each sub-clusters. After these steps, any errors and biases introduced by PCR amplification or sequencing were eliminated.

FACS analysis of the cell cycle

For analysis of cell-cycle distribution, cells were collected 48 h after splitting and were fixed in cold 70% ethanol (−20 °C). After fixation at 4 °C for at least 24 h, cells were stained with propidium iodide, and at least 10,000 cells were analyzed by FACS. Data subsequently were analyzed with FlowJo software.

Statistics and reproducibility

All the statistical data are presented as the mean ± SEM unless indicated otherwise. Each test was repeated at least three times, and the results were analyzed by GraphPad Prism 5 software. Statistical analysis was performed using Student's *t*-test. p values < 0.05 were considered statistically significant. All the experiments were conducted at least three times unless indicated otherwise.

Reporting summary

Further information on research design is available in the Nature Portfolio Reporting Summary linked to this article.

Data availability

All of the RNA-seq data from this study can be accessed with the Gene Expression Omnibus (GEO) code GSE281755, and the Mass spectrometry raw data in this publication are available with the PRIDE code PXD059649. The supplementary Data file includes the source data corresponding to the graphs presented in the main figures and supplemental figures. Uncropped and unedited Western blots are provided in Supplementary Fig. 5. The data that support the findings of this study are available from the corresponding author upon reasonable request.

Received: 8 August 2024; Accepted: 17 January 2025;
Published online: 26 January 2025

References

1. Cavazza, T. et al. Parental genome unification is highly error-prone in mammalian embryos. *Cell* **184**, 2860–2877 e2822 (2021).
2. Palmerola, K. L. et al. Replication stress impairs chromosome segregation and preimplantation development in human embryos. *Cell* **185**, 2988–3007 e2920 (2022).
3. Vanneste, E. et al. Chromosome instability is common in human cleavage-stage embryos. *Nat. Med.* **15**, 577–583 (2009).
4. De Paepe, C., Krivega, M., Cauffman, G., Geens, M. & Van de Velde, H. Totipotency and lineage segregation in the human embryo. *Mol. Hum. Reprod.* **20**, 599–618 (2014).
5. Heyer, B. S., MacAuley, A., Behrendtsen, O. & Werb, Z. Hypersensitivity to DNA damage leads to increased apoptosis during early mouse development. *Genes Dev.* **14**, 2072–2084 (2000).
6. Laurent, A. & Blasi, F. Differential DNA damage signalling and apoptotic threshold correlate with mouse epiblast-specific hypersensitivity to radiation. *Development* **142**, 3675–3685 (2015).
7. Liu, J. C. et al. High mitochondrial priming sensitizes hESCs to DNA-damage-induced apoptosis. *Cell Stem Cell* **13**, 483–491 (2013).
8. Pan, Q., Shai, O., Lee, L. J., Frey, B. J. & Blencowe, B. J. Deep surveying of alternative splicing complexity in the human transcriptome by high-throughput sequencing. *Nat. Genet.* **40**, 1413–1415 (2008).
9. Baralle, F. E. & Giudice, J. Alternative splicing as a regulator of development and tissue identity. *Nat. Rev. Mol. Cell Biol.* **18**, 437–451 (2017).
10. Revil, T., Gaffney, D., Dias, C., Majewski, J. & Jerome-Majewska, L. A. Alternative splicing is frequent during early embryonic development in mouse. *BMC Genom.* **11**, 399 (2010).
11. Tian, G. G., Li, J. & Wu, J. Alternative splicing signatures in preimplantation embryo development. *Cell Biosci.* **10**, 33 (2020).
12. Torre, D. et al. Isoform-resolved transcriptome of the human preimplantation embryo. *Nat. Commun.* **14**, 6902 (2023).
13. Paulsen, R. D. et al. A genome-wide siRNA screen reveals diverse cellular processes and pathways that mediate genome stability. *Mol. Cell* **35**, 228–239 (2009).
14. Olazabal-Herrero, A. et al. The FANCI/FANCD2 complex links DNA damage response to R-loop regulation through SRSF1-mediated mRNA export. *Cell Rep.* **43**, 113610 (2024).
15. He, X. & Zhang, P. Serine/arginine-rich splicing factor 3 (SRSF3) regulates homologous recombination-mediated DNA repair. *Mol. Cancer* **14**, 158 (2015).
16. Do, D. V. et al. SRSF3 maintains transcriptome integrity in oocytes by regulation of alternative splicing and transposable elements. *Cell Discov.* **4**, 33 (2018).
17. Chou, W. C., Jha, S., Linhoff, M. W. & Ting, J. P. The NLR gene family: from discovery to present day. *Nat. Rev. Immunol.* **23**, 635–654 (2023).
18. Akoury, E., Zhang, L., Ao, A. & Slim, R. NLRP7 and KHDC3L, the two maternal-effect proteins responsible for recurrent hydatidiform moles, co-localize to the oocyte cytoskeleton. *Hum. Reprod.* **30**, 159–169 (2015).
19. Li, G. et al. NLRP7 is expressed in the ovine ovary and associated with in vitro pre-implantation embryo development. *Reproduction* **158**, 415–427 (2019).
20. Zhang, P. et al. Expression analysis of the NLRP gene family suggests a role in human preimplantation development. *PLoS ONE* **3**, e2755 (2008).
21. Murdoch, S. et al. Mutations in NALP7 cause recurrent hydatidiform moles and reproductive wastage in humans. *Nat. Genet.* **38**, 300–302 (2006).
22. Hui, P., Buza, N., Murphy, K. M. & Ronnett, B. M. Hydatidiform moles: genetic basis and precision diagnosis. *Annu. Rev. Pathol.* **12**, 449–485 (2017).
23. Kou, Y. C. et al. A recurrent intragenic genomic duplication, other novel mutations in NLRP7 and imprinting defects in recurrent biparental hydatidiform moles. *Mol. Hum. Reprod.* **14**, 33–40 (2008).
24. El-Maarri, O. et al. Maternal alleles acquiring paternal methylation patterns in biparental complete hydatidiform moles. *Hum. Mol. Genet.* **12**, 1405–1413 (2003).
25. Hayward, B. E, et al. Genetic and epigenetic analysis of recurrent hydatidiform mole. *Hum. Mutation* **30**, E629 (2009).
26. Sanchez-Delgado, M. et al. Absence of maternal methylation in biparental hydatidiform moles from women with NLRP7 maternal-effect mutations reveals widespread placenta-specific imprinting. *PLoS Genet.* **11**, e1005644 (2015).
27. Zhang, P. et al. Abnormal processing of IL-1beta in NLRP7-mutated monocytes in hydatidiform mole patients. *Clin. Exp. Immunol.* https://doi.org/10.1111/cei.13472 (2020).
28. Abi Nahed, R. et al. NLRP7 is increased in human idiopathic fetal growth restriction and plays a critical role in trophoblast differentiation. *J. Mol. Med.* **97**, 355–367 (2019).

29. Alici-Garipcan, A. et al. NLRP7 plays a functional role in regulating BMP4 signaling during differentiation of patient-derived trophoblasts. *Cell Death Dis.* **11**, 658 (2020).
30. Ambartsumyan, G. & Clark, A. T. Aneuploidy and early human embryo development. *Hum. Mol. Genet.* **17**, R10–15 (2008).
31. Abi Nahed, R. et al. Role of NLRP7 in normal and malignant trophoblast cells. *Biomedicines* **10**, https://doi.org/10.3390/biomedicines10020252 (2022).
32. Xu, R. H. et al. BMP4 initiates human embryonic stem cell differentiation to trophoblast. *Nat. Biotechnol.* **20**, 1261–1264 (2002).
33. Yang, Y. et al. Heightened potency of human pluripotent stem cell lines created by transient BMP4 exposure. *Proc. Natl Acad. Sci. USA* **112**, E2337–E2346 (2015).
34. Mahadevan, S. et al. NLRP7 affects trophoblast lineage differentiation, binds to overexpressed YY1 and alters CpG methylation. *Hum. Mol. Genet.* **23**, 706–716 (2014).
35. Theunissen, T. W. et al. Systematic identification of culture conditions for induction and maintenance of naive human pluripotency. *Cell Stem Cell* **15**, 471–487 (2014).
36. Yu, L. et al. Blastocyst-like structures generated from human pluripotent stem cells. *Nature* **591**, 620–626 (2021).
37. Bolton, H. et al. Mouse model of chromosome mosaicism reveals lineage-specific depletion of aneuploid cells and normal developmental potential. *Nat. Commun.* **7**, 11165 (2016).
38. Singla, S., Iwamoto-Stohl, L. K., Zhu, M. & Zernicka-Goetz, M. Autophagy-mediated apoptosis eliminates aneuploid cells in a mouse model of chromosome mosaicism. *Nat. Commun.* **11**, 2958 (2020).
39. Li, B. et al. NLRP7 deubiquitination by USP10 promotes tumor progression and tumor-associated macrophage polarization in colorectal cancer. *J. Exp. Clin. Cancer Res.* **40**, 126 (2021).
40. Cargill, M., Venkataraman, R. & Lee, S. DEAD-Box RNA helicases and genome stability. *Genes* **12**, https://doi.org/10.3390/genes12101471 (2021).
41. Sun, Y. et al. PRPF8 controls alternative splicing of PIRH2 to modulate the p53 pathway and survival of human ESCs. *J. Cell. Physiol.* **238**, 1909–1920 (2023).
42. Beli, P. et al. Proteomic investigations reveal a role for RNA processing factor THRAP3 in the DNA damage response. *Mol. Cell* **46**, 212–225 (2012).
43. Ray Chaudhuri, A. & Nussenzweig, A. The multifaceted roles of PARP1 in DNA repair and chromatin remodelling. *Nat. Rev. Mol. Cell Biol.* **18**, 610–621 (2017).
44. Wright, W. D., Shah, S. S. & Heyer, W. D. Homologous recombination and the repair of DNA double-strand breaks. *J. Biol. Chem.* **293**, 10524–10535 (2018).
45. Niakan, K. K., Han, J., Pedersen, R. A., Simon, C. & Pera, R. A. Human pre-implantation embryo development. *Development* **139**, 829–841 (2012).
46. Han, J. et al. NLRP7 participates in the human subcortical maternal complex and its variants cause female infertility characterized by early embryo arrest. *J. Mol. Med.* **101**, 717–729 (2023).
47. Wang, X. et al. Novel mutations in genes encoding subcortical maternal complex proteins may cause human embryonic developmental arrest. *Reprod. Biomed. Online* **36**, 698–704 (2018).
48. Zhang, W. et al. KHDC3L mutation causes recurrent pregnancy loss by inducing genomic instability of human early embryonic cells. *PLoS Biol.* **17**, e3000468 (2019).
49. Wang, E. T. et al. Alternative isoform regulation in human tissue transcriptomes. *Nature* **456**, 470–476 (2008).
50. Munoz, M. J. et al. DNA damage regulates alternative splicing through inhibition of RNA polymerase II elongation. *Cell* **137**, 708–720 (2009).
51. Wang, C. et al. Single-cell analysis of isoform switching and transposable element expression during preimplantation embryonic development. *PLoS Biol.* **22**, e3002505 (2024).
52. Li, J. et al. Rbm14 maintains the integrity of genomic DNA during early mouse embryogenesis via mediating alternative splicing. *Cell Prolif.* **53**, e12724 (2020).
53. Matveeva, E. et al. Involvement of PARP1 in the regulation of alternative splicing. *Cell Discov.* **2**, 15046 (2016).

Acknowledgements

This work was supported by the Science and Technology Program of Guizhou Province (grant number: ZK[2021]121, CXTD[2023]018), a Scientific research project of Higher education institution, Department of Education of Guizhou Province (grant number: [2022]189), the National Natural Science Foundation of China (grant no. 82060151) and the university-level key laboratory construction project of Guizhou Medical University (No. [2024]002). We gratefully acknowledge Dr. Tianqing Li (Kunming University of Science and Technology) for providing the H9 ESCs line. We thank Dr. Xianbin Wang (Guizhou Medical University) for RNA-seq data analysis in this work. We also thank Dr. Zinian Wang (Guizhou Medical University) for his advice on the revision of the manuscript.

Author contributions

Z.L.C., L.X.J., L.Z.C., and P.L. designed the experiments. Z.L.C. and L.X.J. performed most of the experiments. M.S. and Q.B.Z. participated in the data analysis and discussions of the study. L.Z.C. and P.L. wrote the paper. All authors read and approved the final manuscript.

Competing interests

The authors declare no competing interests.

Additional information

Supplementary information The online version contains supplementary material available at https://doi.org/10.1038/s42003-025-07571-5.

Correspondence and requests for materials should be addressed to Peng Luo or Liangzhao Chu.

Peer review information *Communications Biology* thanks Maria Krivega, Hannah Demond and the other, anonymous, reviewer(s) for their contribution to the peer review of this work. Primary Handling Editors: Joanna Timmins and Mengtan Xing.